New Applications of X-ray Tomography in Pyrolysis of Biomass: Biochar Imaging

Keith Jones [†,§], Girish Ramakrishnan[†], Minori Uchimiya[‡], Alexander Orlov[†,*]

[†]*Department of Material Science and Engineering, State University of New York, Stony Brook, New York 11794*

[§]*Environmental and Climate Sciences Department, Brookhaven National Laboratory, Upton, NY 11973-5000*

[‡]*USDA-ARS Southern Regional Research Center, 1100 Robert E. Lee Boulevard, New Orleans, Louisiana 70124*

[*] *Corresponding author Telephone: +1-631-632-9978 email: alexander.orlov@stonybrook.edu*

Accepted for publication in
Energy & Fuels
(January 2015)

ABSTRACT

We report on the first ever use of non-destructive micrometer-scale synchrotron-computed microtomography (CMT) for biochar material characterization as a function of pyrolysis temperature. This innovative approach demonstrated an increase in micron-sized marcropore fraction of the Cotton Hull (CH) sample, resulting in up to 29% sample porosity. We have also found that initial porosity development occurred at low temperatures (below 350°C) of pyrolysis, consistent with chemical composition of CH. This innovative technique can be highly complementary to traditional BET measurements, considering that Barrett-Joyner-Halenda (BJH) analysis of pore size distribution cannot detect these macropores. Such information can be of substantial relevance to environmental applications, given that water retention by biochars added to soils is controlled by macropore characteristic among the other factors. Complementing our data with SEM, EDX and XRF characterization techniques allowed us to develop a better understanding of evolution of biochar properties during its production, such presence of metals and initial morphological features of biochar before pyrolysis. These results have significant implications for using biochar as a soil additive and for clarifying the mechanisms of biofuel production by pyrolysis.

KEYWORDS

Biochar, biofuel, pyrolysis, microtomography, porosity

INTRODUCTION

This work is focused on new applications of non-destructive micrometer-scale synchrotron computed microtomography (CMT) to observe pyrolysis of biomass, which is of substantial relevance for energy and environmental applications. Biochar is produced by high temperature treatment of biomass (300-500°C and above) in the absence of oxygen (pyrolysis). This treatment results in a product (biochar) comprising primarily of organic carbon[1, 2]. This approach allows agricultural industry to reduce its carbon footprint by storing pyrolyzed biomass in soil with an estimated residence time ranging from 5-29 years to 1,300-2,600 years depending on references cited [3, 4]. In addition, there are other benefits from the study of biochar properties. For example, biochar is a by-product of biofuel production and mechanistic knowledge of biochar formation can be invaluable in understanding the chemical pathways of biofuel production.

Among many physicochemical parameters of biochar, it is important to single out porosity as it has a significant influence on water retention and adsorption properties. Although some porosity is naturally present in biomass, most of it comes from removal of various organic constituents of biomass that have variable temperature stability[5, 6]. Together with specific surface area, porosity plays a major role in predicting water retention by biochar and can also aid in understanding of water adsorption and desorption behavior[7]. Computed tomography (CT) offers a very unique insight into such behavior. There are already a number of studies on using CT to image geological and soil samples[8-10]. For example, a recent study of soils where biochar was added resulted in pore size reduction of the soil sample, contributing to a better water retention[11, 12]. Although no published work followed biochar pyrolysis trends with CT, there was a recent work

on pyrolysis of oil shale. Using CT the authors were able to image three-dimensional pore network structure developed due to pyrolysis, which was coupled with lattice Boltzmann simulation of flow through the pore network[8]. In this paper we present the first ever application of 3D X-ray synchrotron based computed microtomography (CMT) to elucidate the pore structure development of biochars. Given the spatial resolution of CMT this paper primarily focuses on macropores in the micrometer range, although smaller mesopores (<50nm) and nanopores (<2nm) are also expected during the pyrolysis[5]. This is an important pore size range, especially for water retention and release[11, 12]

MATERIALS AND METHODS

Cottonseed hulls (hereby denoted CH) were pyrolyzed at 25, 350, 500, 650 and 800 °C for 4 h under 1600 mL min^{-1} N_2 flow rate using a laboratory scale box furnace (22 L void volume) with a retort (Lindberg, Type 51662HR, Watertown, WI). The resulting chars (CH25, CH350, CH500, CH650 and CH800) were allowed to cool to room temperature overnight under N_2 atmosphere.

Samples were scanned using 3D X-ray Computed Micro Tomography (CMT) at the X2B beam line at the National Synchrotron Light Source at Brookhaven National Laboratory. The apparatus uses a 1340 x 1300 pixel CCD camera with a pixel size of 4μm to acquire radiographs of the sample using a CsI area x-ray detector. A total of 1200 radiographs were acquired as the sample was rotated through 180°. The results were converted into a tomographic volume and visualized using open-source software. The results give a 3-dimensional view of the linear attenuation coefficients for each voxel. The linear attenuation coefficient is defined by the mass attenuation

coefficient in cm^2/g times the material density. The x-ray energy used for the work was 12.9 keV. Metal contents of the materials were also investigated using micro x-ray fluorescence (XRF) techniques at NSLS beam line X27A. The beam size was 10 μm.

The Scanning Electron Microscopy (SEM) images, which also included elemental analysis, were obtained using Field Emission Scanning Electron Microscope (SEM) LEO Gemini 1550 equipped with Schottky Field Emission gun (20 KV) and a Robinson backscatter detector. The samples were coated with gold for 20 seconds using the low vacuum sputter coater to prevent charging.

RESULTS AND DISCUSSION

A 3D CMT reconstruction of unpyrolyzed cottonseed hull (CH) is shown in Figure 1-A. This reconstruction is representative of a CH fragment used in our experiments. In addition to scale bar, the image also has X-ray attenuation color scale, which can be used to study porosity development during the pyrolysis as illustrated below. For reference purposes we also included the SEM image of CH. An important advantage of 3D CMT as compared to SEM is a CMT capability to image multiple cross sections of the sample in a non-destructive way. A cross section of the unpyrolyzed sample is presented in Figure 2-A. It indicates that the untreated sample does not have significant porosity, although given that the resolution of the technique is on μm scale, smaller pores would not be revealed by the CMT measurements. In contrast to the untreated sample, a dramatic increase in porosity due to pyrolysis is revealed in the cotton hull cross section taken after pyrolysis at 650°C displayed in Figure 2-B. It is also important to note

that the most significant development of porosity occurs at lower temperatures of pyrolysis, as obvious from comparison of 350°C pyrolyzed samples (Figure 2-C) and 500°C pyrolyzed sample (Figure 2-D). As soon as the outer layer is removed at temperatures of around 800°C, the samples tend to disintegrate into small pieces (Figure 2-F). These dramatic changes in the structures are caused by the destruction and vaporization of specific components of the cotton hull that have different temperature stability. In general the components of biomass include such constituents as cellulose, hemicellulose and lignin[13]. Hemicellulose can decompose at temperatures around 150-350°C, while cellulose will be degraded at 280-350°C[14, 15]. The most stable component, lignin, will undergo the chain fragmentation at around 300-480°C[16]. In case of CH, it primarily consists of cellulose with a minor presence of lignin compounds[17, 18], the most significant development of porosity occurs at temperatures below 400°C as indeed observed in Figure 2. From another perspective, CH can be described in terms of labile and more recalcitrant to microbial degradation carbon fractions[19]. In our previous work[6] we have determined that pyrolysis of CH between 200-800°C resulted in increased fixed carbon from 22.7 to 77.1 wt.% which was accompanied with a decrease in labile carbon. A more detailed information on increase in fixed carbon and ash content, and decrease in volatile matter content are shown in supplementary information (Tables 1 & 2) This is also consistent with our previous work on in-situ characterization of pyrolysis with DRIFTS, where the greatest change in surface functionalities was observed in 200-500°C pyrolysis temperature range[6]. It is important to mention that development of stable graphitic (recalcitrant) structure of carbon during the pyrolysis is intimately linked to the chemical composition of biomass, although there is a scientific debate about the role of mineral content in forming porous structures and the sensitivity of the biochar structure development to the original composition of biomass[20].

Figure 3 shows the linear attenuation coefficients for CH pyrolyzed at different temperatures. The x-ray linear attenuation coefficient, μ, is defined by the equation $I/I_0 = e^{-\mu x}$, where x is distance traversed by the x-ray. It is dependent on the elemental composition of the material and measures the variability of the CH composition on a micrometer size scale. This capability gives new insights into the values found from conventional macroscopic analytical techniques. The plot shows a well-defined peak for the solid material at a value of $2.45 cm^{-1}$ for the CH prior to pyrolysis. We estimated the X-ray mass attenuation coefficient expected for CH material taken as C(45.8%), H(5.5%), O(40.3%), Mg(2.09%), P(0.32%), K(4.26%), Na(0.02%), and Ca(1.75%) using tables from the National Institute of Standards and Technology[21]. In addition, measured concentrations for the heavy elements are given in the supplemental material. The density of cotton hull was taken as $0.19 g/cm^3$. As mentioned above, the calculated linear attenuation coefficient (cm^{-1}) is just the product of the two factors: the x-ray mass attenuation coefficient and the density. The calculated value is about 30% higher than the measured value. The agreement is excellent considering the uncertainties in the factors entering into the calculated result. The attenuation from the metals is roughly equal to the attenuation from the organic materials and is found throughout the measured mass of the CH.

The effect of pyrolysis is to broaden the measured attenuation distribution to both higher and lower values. The increase in the higher values comes from an increase in the concentrations of the heavy elements (See Supplemental material) combined with any increase in density of the materials caused by the pyrolysis. The increase in lower values can mainly be ascribed to loss of organic materials and the associated increase in porosity and the corresponding decrease in bulk

density. Of course, changes in the metal distributions are also possible. Extension of the XRF mapping to measurements on these sections of the CH pyrolyzed material is necessary to clarify this question.

Detailed estimates of the microscale porosity of the materials were made by fitting the peaks attributed to porous and solid regions (Figure 4). The results indicate a dramatic increase in the porosity as a result of increase in pyrolysis temperature. Whereas the section at the beginning of pyrolysis showed no porosity, the sample pyrolyzed at 800°C showed 29% porosity. Importantly, there was a dramatic increase in porosity at the low temperatures following the sequence, whereas at higher temperature the porosity remained relatively stable: (1) unpyrolyzed sample having no porosity; (b) sample pyrolyzed at 350 °C sample having the porosity of 0.27; (c) sample pyrolyzed at 500 °C having porosity of 0.23; (d) sample pyrolyzed at 800 °C having porosity of 0.29. Our data demonstrate that at the beginning of pyrolysis the heat treatment results in the creation of macropore content in the biochar. This is an important result for two reasons. First, conventional BET measurements and pore size calculations using, for example, BJH method do not detect the macropores. It is instructive to mention that for the porosity calculated from pycnometry data, the published data indicate that overall porosity (e.g. for hazelnut shell and douglas fir) remains stable above 370 °C heating temperature[22]. This was attributed to stable fraction of macropores, which we also observed. The only porosity increasing above that temperature is related to nanopores formation, which contribute only a small fraction to the overall porosity. Second, since water retention by biochars in soils is controlled by the macropores (among other parameters such as hydrophilicity of the surface), application of tomography will be a powerful analytical method in the future, especially in the size range

178 (micron size macropores) which other techniques do not cover. Given a capability of 3D
179 reconstruction of pore interconnectivity, comprehensive modeling efforts can be capable of
180 providing unprecedented level of details for understanding water transport and retention.
181
182 The metal content of the CH was explored using both synchrotron XRF and SEM-EDX
183 techniques. The synchrotron work was done at the NSLS X26A beam line. The apparatus is not
184 instrumented for detection of the very light elements such as C, N, and O. For this reason,
185 measurements were also made with the SEM-EDX equipment that was optimized for light
186 element detection. Results from the synchrotron measurement (Supplementary Info Figure S1)
187 indicate a significant presence of metals, including Mn, Fe, Ca, K, Ni, Cu and Zn. It is important
188 to mention that XRF mapping of individual elements in a grain-scale biochar sample
189 (Supplementary Info Figure S2) indicated that there is a significant heterogeneity in the spatial
190 distribution of these metals. This suggests the need for further work to map the distributions on
191 metals within the samples, especially for the sections where there is the most preserved solid
192 structure. Given the significant number of possible mineral phases in biochar[23], further work
193 might also be need to identify some of those phases given the importance of mineral content in
194 pore forming structures. The special heterogeneity in chemical composition might explain some
195 discrepancy in type of metals identified by XRF (Supplementary Info Figure S1) and SEM
196 (Supplementary Info Figure S3), which is also complemented by analysis of total elemental
197 content[24] determined by microwave digestion and EDTA extraction (Supplementary Info Table
198 S1).
199

The SEM results (Figure 4A-D) of the unpyrolyzed sample showed a presence of surface associated pores, which were not obvious in the CMT results (Figure 2-A). The reason for detecting these pores is based on higher resolution of the SEM technique, which is measured in nanometers rather than micrometers for CMT. Moreover, the SEM images surface structures whereas CMT shows cross section of the samples. Although SEM technique has been well established for characterizing biochars[25], it was noted that observing trends in porosity development strongly depends on biochar preparation conditions[5]. Indeed the images of pyrolyzed samples (Figure 4E-H) did not reveal a consistent trend in porosity development, possibly due to the above mentioned fact that only the surface of the sample was imaged as compared to sample cross-sections (Figure 2) obtained by CMT. This lack of observed trends is also consistent with published work on pyrolysis of sawdust where the samples prepared without a prolonged temperature holding time did not demonstrate a clear trend in porosity observed in SEM images[5]. The same work also suggests that porosity can be adjusted by tuning the biochar preparation conditions, such as introduction of fast pyrolysis[5, 26]. Finally, the EDX analysis of elemental composition (Supplementary Info Figure S3) appeared to be not as sensitive as that of XRF analysis by synchrotron based technique, as obvious from the fact that fewer metals were detected in the sample (e.g. K, Mg and Ca). As discussed earlier, this is consistent with SEM being more sensitive to alkali and alkaline earth metals as compared to XRF. In addition, this discrepancy can be also attributed to a very heterogeneous nature of the samples, as analysis depth and analysis spots were different for SEM and XRF techniques.

CONCLUSIONS

The results of CMT, SEM, EDX and XRF analysis of biochar samples presented in this publication illustrate the very important advantage of adding CMT-based image analysis to the usual analytical techniques since it is it gives a refined understanding of porosity development in biochar. This is critical in obtaining refined understanding of both fundamental and applied aspects of biomass pyrolysis. We believe that this first ever demonstration of using synchrotron-based CMT techniques for biochar imaging has significant importance for both environmental and biofuels research areas.

AUTHOR INFORMATION

Corresponding Author

Telephone: +1-631-632-9978. Email: alexander.orlov@stonybrook.edu

Notes

The authors declare no competing financial interest.

ACKNOWLEDGEMENTS

Work supported in part by the U. S. Department of Energy under contract No: DE-AC02-98CH10886. The U.S. DOE, Office of Science, and Office of Basic Energy Sciences supported use of National Synchrotron Light Source.

ASSOCIATED CONTENT

Supporting Information

Additional information as noted in the text. This information is available free of charge via the Internet at http://pubs.acs.org.

247 FIGURES

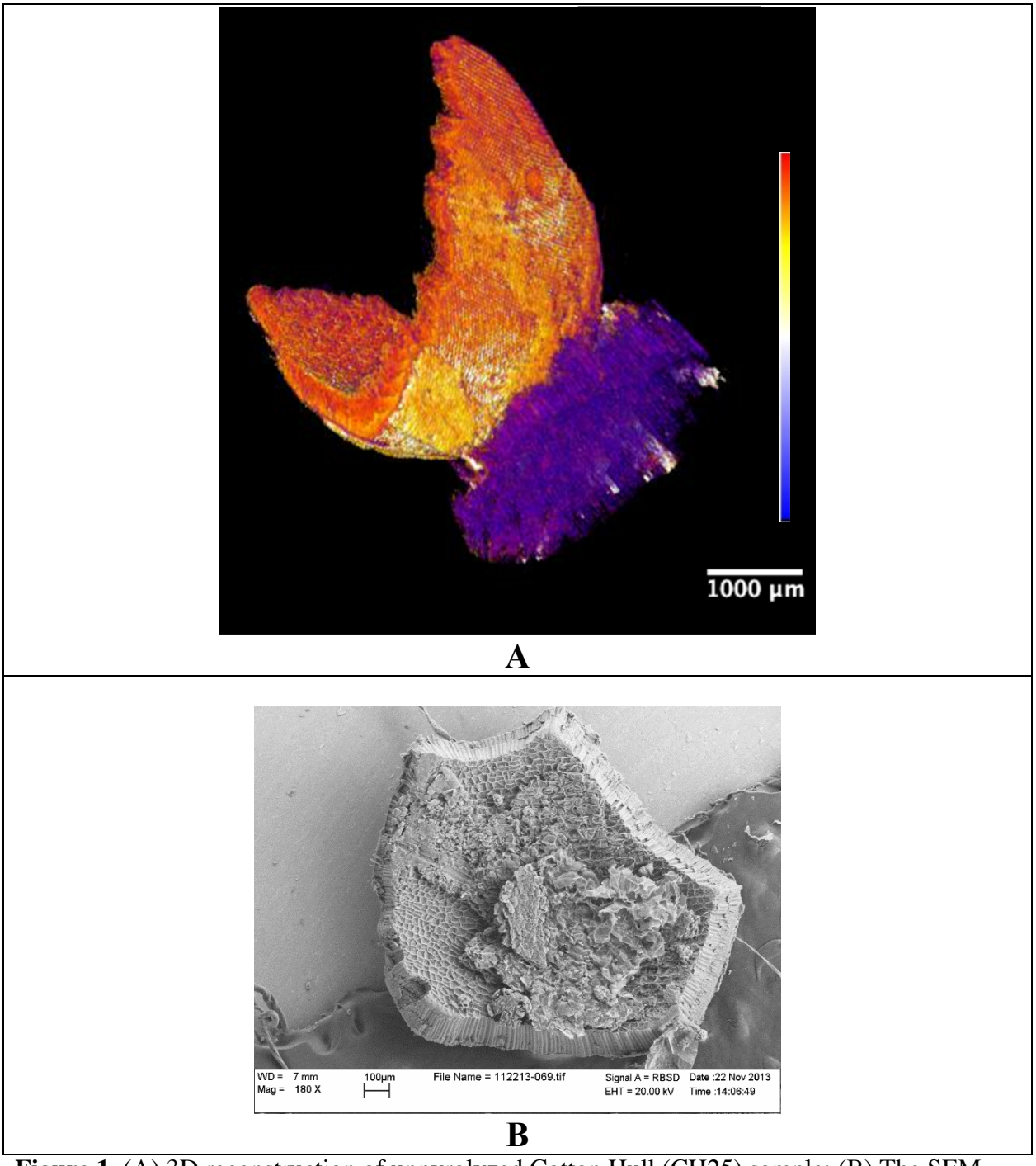

248 **Figure 1.** (A) 3D reconstruction of unpyrolyzed Cotton Hull (CH25) sample; (B) The SEM
249 image of CH25 described later in the text.

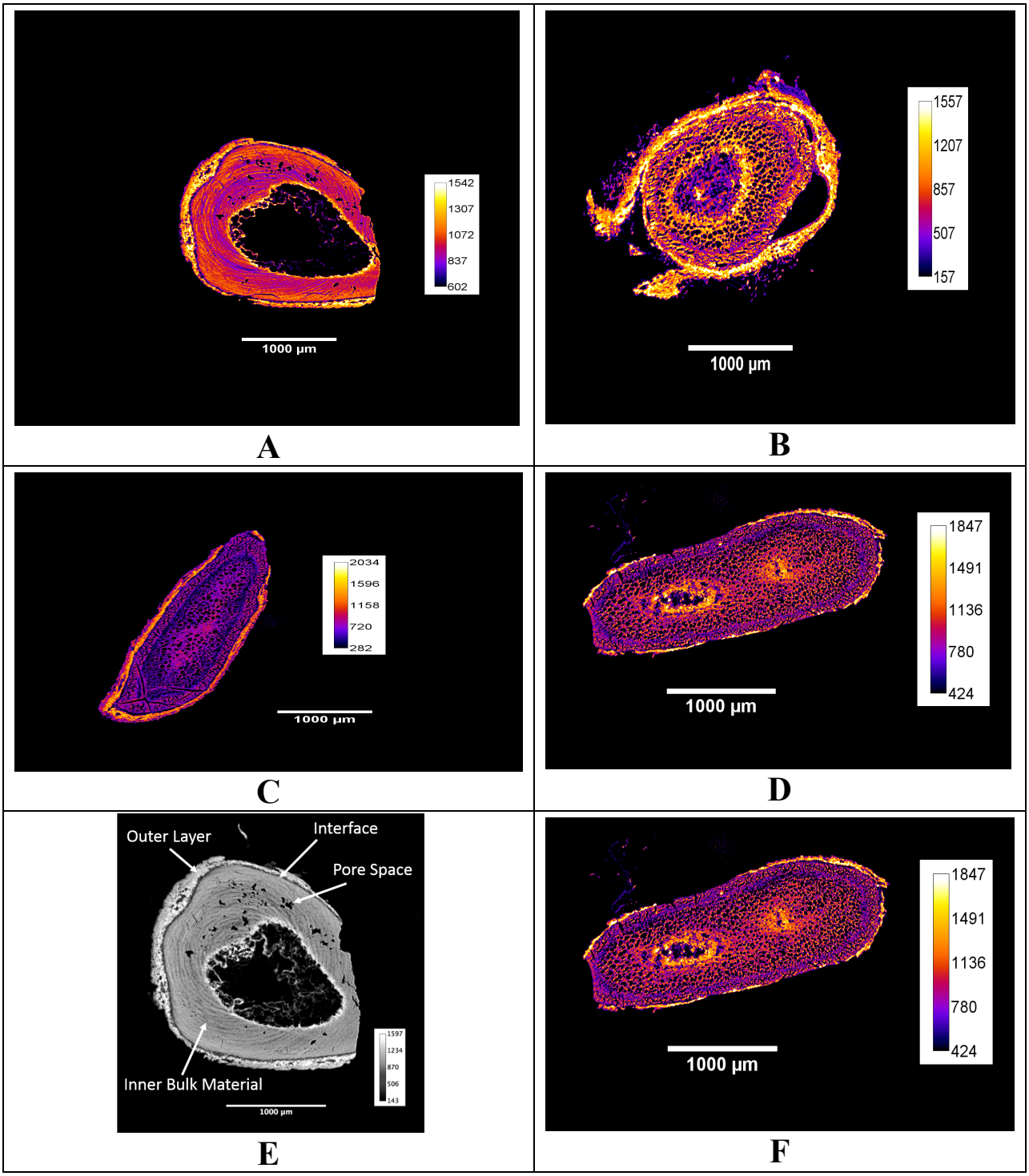

Figure 2. Cotton Hull samples: (A) unpyrolyzed; (B) pyrolyzed at 650 °C, (C) pyrolyzed at 350 °C; (D) pyrolyzed at 500 °C; (E) unpyrolyzed outlining different cotton hull morphology; (F) pyrolyzed at 800 °C showing disintegration of the sample.

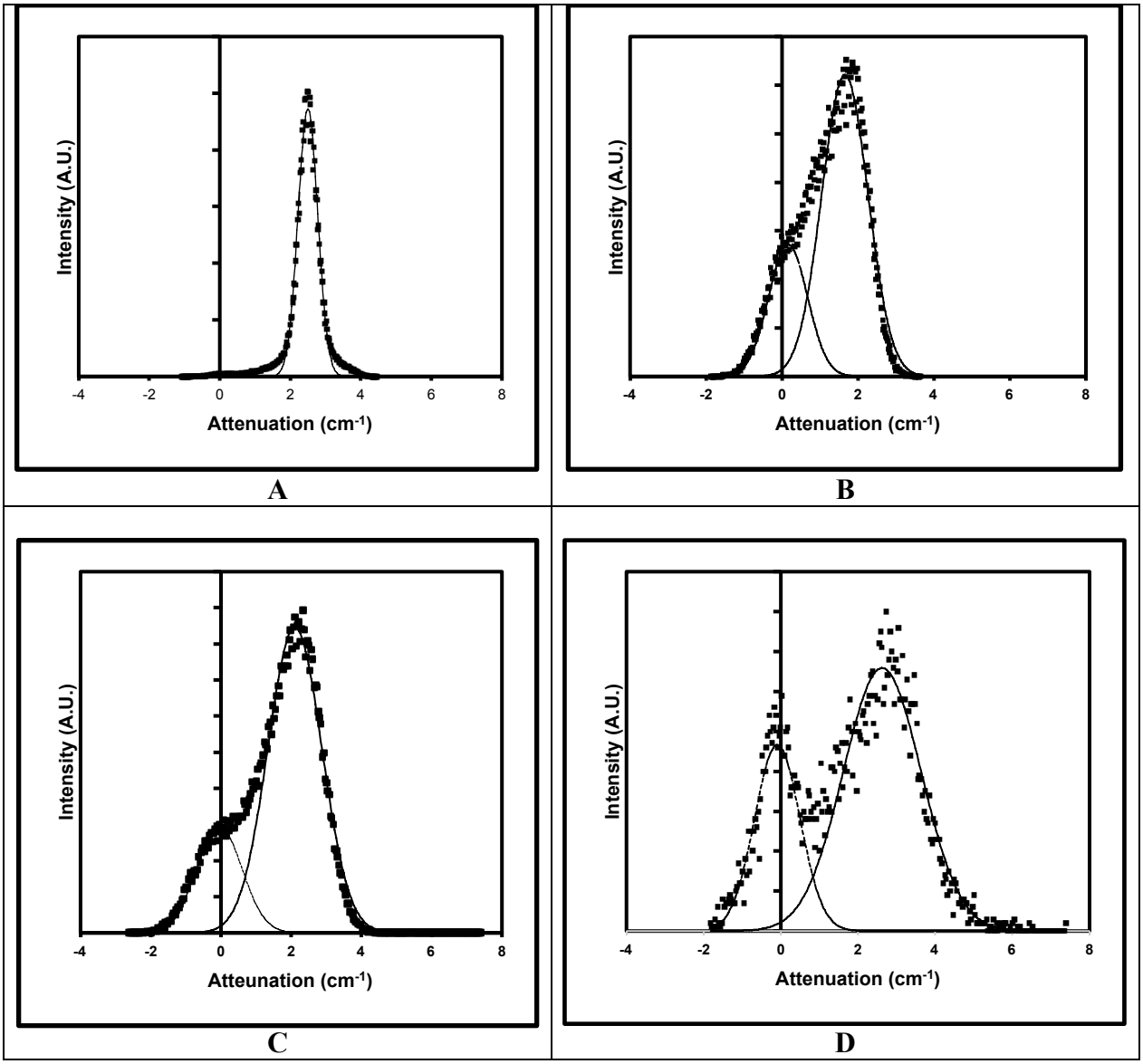

Figure 3. Attenuation of Cotton Hull pyrolyzed at different temperatures: (A) unpyrolyzed; (b) pyrolyzed at 350 °C, the porosity is 0.27; (c) pyrolyzed at 500 °C, the porosity is 0.23; (d) pyrolyzed at 800 °C, the porosity is 0.29.

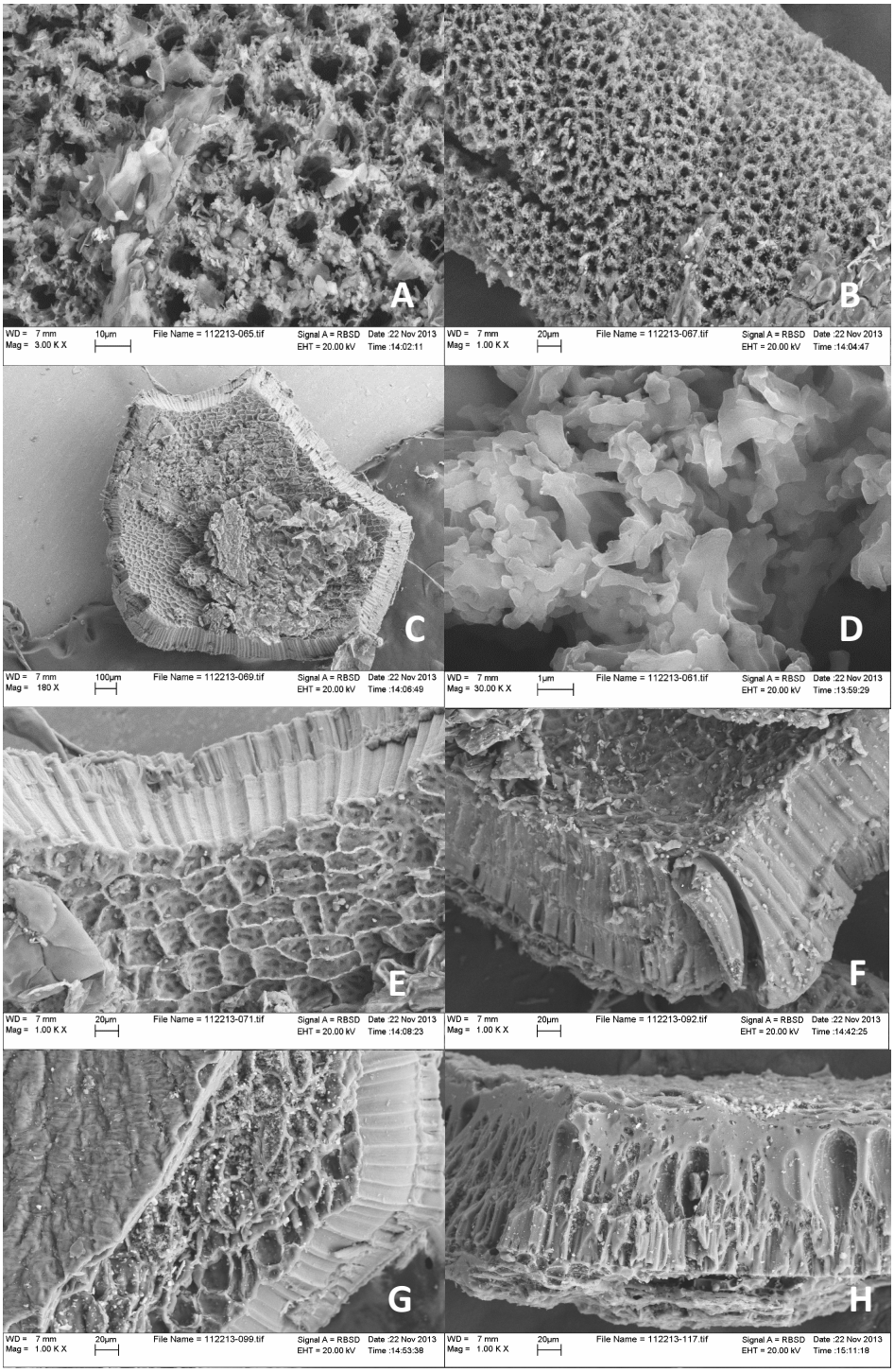

Figure 4. The SEM images of Cotton Hull (A-D) showing unpyrolyzed at different magnifications and (E-H) showing pyrolyzed at different temperatures (E) Unpyrolyzed, (F) Pyrolyzed at 350°C, (G) Pyrolyzed at 500°C, and (H) Pyrolyzed at 800°C.

TABLES

Char	C, % (w/w)	H, % (w/w)	N, % (w/w)	S, % (w/w)	O, % (w/w)	H/C molar ratio	O/C Molar ratio	BET SA, m^2/g	Micropore area, m^2/g
CH25	51±2	6.6±0.3	0.7± 0.1	1.03±0.05	41±2	1.5±0.1	0.6±0.1	n.d.	
CH200	51.9±0.5	6.0±0.1	0.60± 0.04	0.99±0.01	40.5±0.4	1.38±0.02	0.59±0.01	n.d.	
CH350	77±1	4.53±0.05	1.9±0.4	0.8±0.1	15.7±0.04	0.70±0.01	0.153±0.001	4.7±0.8	
CH500	87.5±0.1	2.82±0.02	1.5±0.1	0.50±0.01	7.6±0.2	0.385±0.003	0.065±0.002	0	
CH650	91.0±0.4	1.26±0.02	1.6±0.1	0.26±0.03	5.9±0.3	0.166±0.002	0.049±0.003	34±3	0.007±0
CH800	90±1	0.6±0.1	1.9±0.1	0.16±0.03	7±1	0.08±0.01	0.06±0.01	322±1	274±1

Table 1: Elemental Composition, Molar Ratio, and BET Surface Area for Cottonseed Hull Chars. Values are given as mean (standard deviation for triplicate (elemental composition) or duplicate (BET surface area) measurements. Elemental composition and molar ratio are given on a moisture- and ash-free basis

Char	yield,[b] % (w/w)	moisture, % (w/w)	VM,[c] % (w/w)	fixed C,[d] % (w/w)	ash,[c] % (w/w)	0.1 M HCl washing, % wt loss[e]	pH[e]	pH_{pzc}
CH200	83.4±0.8	5.3 ± 0.2	69.3±0.2	22.3±0.1	3.1±0.1	4.3	3.7	3.5
CH350	36.8±0.1	6.81 ± 0.01	34.9±0.1	52.6±0.2	5.7±0.1	6.6	6.9	7.0
CH500	28.9±0.1	6.53 ± 0.01	18.6±0.6	67.0±0.7	7.9±0.1	5.7	8.5	10.1
CH650	25.4±0.2	8.21 ± 0.02	13.27±0.04	70.3±0.2	8.3±0.2	9.7	8.6	9.9
CH800	24.2±0.6	9.92 ± 0.05	11.42±0.1	69.49±0.01	9.2±0.1	8.6	7.7	9.2

[a]Proximate analysis results are given as mean (standard deviation for duplicate measurements. [b]Mean (SD for replicate production. [c]Moisture-free values. [d]Calculated by difference after moisture, VM, and ash measurements. [e]After 0.1 M HCl washing.

Table 2: Yield and Moisture, Volatile Matter (VM), Fixed Carbon and Ash Contents, pH, and pH_{pzc} of Cottonseed Hull Chars[a].

REFERENCES

1. Keiluweit, M.; Nico, P. S.; Johnson, M. G.; Kleber, M., Dynamic molecular structure of plant biomass-derived black carbon (biochar). *Environmental Science & Technology* **2010,** 44, (4), 1247-1253.
2. Shinogi, Y.; Kanri, Y., Pyrolysis of plant, animal and human waste: Physical and chemical characterization of the pyrolytic products *Bioresource Technology* **2003,** 90, (3), 241-247.
3. Lehmann, J.; Skjemstad, J.; Sohi, S.; Carter, J.; Barson, M.; Falloon, P.; Coleman, K.; Woodbury, P.; Krull, E., Australian climate-carbon cycle feedback reduced by soil black carbon. *Nature Geoscience* **2008,** 1, (12), 832-835.
4. Steinbeiss, S.; Gleixner, G.; Antonietti, M., Effect of biochar amendment on soil carbon balance and soil microbial activity. *Soil Biology & Biochemistry* **2009,** 41, (6), 1301-1310.
5. Shaaban, A.; Se, S.-M.; Dimin, M. F.; Juoi, J. M.; Mohd Husin, M. H.; Mitan, N. M. M., Influence of heating temperature and holding time on biochars derived from rubber wood sawdust via slow pyrolysis. *Journal of Analytical and Applied Pyrolysis* **2014,** 107, (0), 31-39.
6. Uchimiya, M.; Orlov, A.; Ramakrishnan, G.; Sistani, K., In situ and ex situ spectroscopic monitoring of biochar's surface functional groups. *Journal of Analytical and Applied Pyrolysis* **2013,** 102, 53-59.
7. Lattao, C.; Cao, X. Y.; Mao, J. D.; Schmidt-Rohr, K.; Pignatello, J. J., Influence of Molecular Structure and Adsorbent Properties on Sorption of Organic Compounds to a Temperature Series of Wood Chars. *Environmental Science & Technology* **2014,** 48, (9), 4790-4798.
8. Tiwari, P.; Deo, M.; Lin, C. L.; Miller, J. D., Characterization of oil shale pore structure before and after pyrolysis by using X-ray micro CT. *Fuel* **2013,** 107, 547-554.
9. Ketcham, R. A.; Carlson, W. D., Acquisition, optimization and interpretation of X-ray computed tomographic imagery: applications to the geosciences. *Computers & Geosciences* **2001,** 27, (4), 381-400.
10. Ojeda-Magana, B.; Quintanilla-Dominguez, J.; Ruelas, R.; Tarquis, A. M.; Gomez-Barba, L.; Andina, D., Identification of pore spaces in 3D CT soil images using PFCM partitional clustering. *Geoderma* **2014,** 217, 90-101.
11. Devereux, R. C.; Sturrock, C. J.; Mooney, S. J., The effects of biochar on soil physical properties and winter wheat growth. *Earth and Environmental Science Transactions of the Royal Society of Edinburgh* **2012,** 103, (1), 13-18.
12. Quin, P. R.; Cowie, A. L.; Flavel, R. J.; Keen, B. P.; Macdonald, L. M.; Morris, S. G.; Singh, B. P.; Young, I. M.; Van Zwieten, L., Oil mallee biochar improves soil structural properties—A study with x-ray micro-CT. *Agriculture, Ecosystems & Environment* **2014,** 191, (0), 142-149.
13. Rezaei, P. S.; Shafaghat, H.; Daud, W. M. A. W., Production of green aromatics and olefins by catalytic cracking of oxygenate compounds derived from biomass pyrolysis: A review. *Applied Catalysis A* **2014,** 469, 490-511.
14. Brebu, M.; Vasile, C., Thermal Degradation of Lignin - a Review. *Cellulose Chemistry and Technology* **2010,** 44, (9), 353-363.
15. Varhegyi, G.; Antal, M. J.; Szekely, T.; Szabo, P., Kinetics of the Thermal-Decomposition of Cellulose, Hemicellulose, and Sugar-Cane Bagasse. *Energy & Fuels* **1989,** 3, (3), 329-335.
16. Bahng, M.-K.; Donohoe, B. S.; Nimlos, M. R., Application of an Fourier Transform-Infrared Imaging Tool for Measuring Temperature or Reaction Profiles in Pyrolyzed Wood. *Energy & Fuels* **2011,** 25, 370-378.

17. Garleb, K. A.; Fahey, G. C.; Lewis, S. M.; Kerley, M. S.; Montgomery, L., Chemical - Composition and Digestibility of Fiber Fractions of Certain by-Products of Feedstuffs Fed to Ruminants. *Journal of Animal Science* **1988,** 66, (10), 2650-2662.
18. Himmelsbach, D. S.; Hellgeth, J. W.; McAlister, D. D., Development and use of an attenuated total reflectance/Fourier transform infrared (ATR/FT-IR) spectral database to identify foreign matter in cotton. *Journal of Agricultural and Food Chemistry* **2006,** 54, (20), 7405-7412.
19. Zimmerman, A. R., Abiotic and Microbial Oxidation of Laboratory-Produced Black Carbon (Biochar). *Environmental Science & Technology* **2010,** 44, (4), 1295-1301.
20. Meszaros, E.; Jakab, E.; Varhegyi, G.; Bourke, J.; Manley-Harris, M.; Nunoura, T.; Antal, M. J., Jr., Do all carbonized charcoals have the same chemical structure? 1. Implications of thermogravimetry - Mass spectrometry measurements. *Industrial & Engineering Chemistry Research* **2007,** 46, (18), 5943-5953.
21. Reference data from the National Institute of Standards and Technology http://physics.nist.gov/PhysRefData/Xcom/html/xcom1.html
22. Gray, M.; Johnson, M. G.; Dragila, M. I.; Kleber, M., Water uptake in biochars: The roles of porosity and hydrophobicity. *Biomass & Bioenergy* **2014,** 61, 196-205.
23. Vassilev, S. V.; Baxter, D.; Andersen, L. K.; Vassileva, C. G., An overview of the composition and application of biomass ash. Part 1. Phase-mineral and chemical composition and classification. *Fuel* **2013,** 105, 40-76.
24. Uchimiya, M.; Hiradate, S., Pyrolysis Temperature-Dependent Changes in Dissolved Phosphorus Speciation of Plant and Manure Biochars. *Journal of Agricultural and Food Chemistry* **2014,** 62, (8), 1802-1809.
25. Chia, C. H.; Gong, B.; Joseph, S. D.; Marjo, C. E.; Munroe, P.; Rich, A. M., Imaging of mineral-enriched biochar by FTIR, Raman and SEM-EDX. *Vibrational Spectroscopy* **2012,** 62, 248-257.
26. Jiang, J.; Zhang, L.; Wang, X.; Holm, N.; Rajagopalan, K.; Chen, F.; Ma, S., Highly ordered macroporous woody biochar with ultra-high carbon content as supercapacitor electrodes. *Electrochimica Acta* **2013,** 113, 481-489.

For Table of Contents Only (TOC Graphic)